F.S.A.I., Vol. 8, Nos. 1–3, pp. 65 – 77, 2002

Toward a Diagnosis System using Nuclear Medicine Image Processing

Mihaela Costin*, Marius Zbancioc*, Adrian Ciobanu*, Cipriana Ştefănescu**

*Computer Science Institute, Romanian Academy, Iaşi
**Medicine and Pharmacy University "Gr. T. Popa", Iaşi

Abstract: The 3D rendering volume [1], [2] is constructed by the help of two N-slices sets, [3], [4] each of them $N \times N$ dimensioned, taking into account an illumination model. One of the sets consists of horizontal images; the other one is a vertical reconstructed images set. In fact, in a SPECT acquisition the images are reconstructed on different axis for example sagittal, coronal and transversal slices.
In order to detect the interest diagnosis areas, fuzzy variable threshold segmentation method is used. On these interest areas non-symmetry gliom may be automatically detected in 2D dimension for each slice and then the 3D representation may be done by a volume-based method. For each volume, 5 projections of voxels arrays are achieved (left lateral, right lateral, anterior, posterior, vertex). Suggestive images are obtained if the edge pixel position [5], [6] is retained into a depth matrix to establish the light intensity in order to shadow it. This method may be applied in tele-medicine diagnosis, too.
Key words: Nuclear medicine, automatic medical image processing, 3D rendering volume reconstruction, fuzzy variable threshold segmentation method, non-symmetry gliom detection volume based methods.

1. Introduction

Medical imaging technology is rapidly expanding and the role of each modality is being constantly redefined [7-9]. Nuclear medicine is a medical image discipline using gamma radiation detection emitted from certain organs pointed by the vector molecules marked with an appropriate radioisotope [10,11]. It mainly plays a significant role in the diagnosis staging [12] and follow-up of patients with cancer [13], [7], [14]. Automatic medical image processing is a field in full expansion [1], [6] due to the need of vital diagnosis in extremely severe cases, when the intervention is to be done in maximum some hours after a cerebral commotion for example. The computer assistance in those cases is essential and a surgical intervention on the brain, made under 6 hours after the accident may completely recover the vital functions [15].

In the first part general principles of different medical imaging processes and technologies are presented. 2D sections and 3D re-constructions by different methods are discussed [1], [2]. In order to emphasize the certainty of diagnosis, as a tool supporting human decision, the non-functional or partial-functioning areas are evidenced.

A statistical situation is detected by the co-occurrence method [16]. The non-functional area is selected and a 3D reconstruction is done.

For the diagnosis the volume in voxels [1] and the degree or the radiopharmaceutical fixation in percents is very important. Our method furnishes these data in order to facilitate the brain Nuclear Medicine (**NM**) diagnosis.

Nowadays more types of body medical imaging: X-ray CT scanner, Magnetic Resonance Imaging (MRI), PET (Positron Emission Tomography), SPECT (Single Photon Emission Computer Tomography) are used in medical routine and produce images of 2D slices of the human body [7-9].

Comparing classical techniques we may say that:

1. Computed Tomography (**CT**) relies on attenuation of X-ray photons by tissue density;

2. Ultrasonography (**US**) relies on the reflection of high frequency sound waves on tissue planes;

3. Magnetic Resonance Imaging (**MRI**) relies on radio-frequency signals from tissues in magnetic fields.

4. The Nuclear Medicine (**NM**) - by emission detection, which is different by principle and its continuous improving perspectives:

The basic principles of **PET** and **SPECT** are based on the detection of photons emitted from the patient. Practically, the potential variety of radiopharmaceuticals or radiotracers is unlimited [7], this providing nuclear imaging techniques with a significant advantage and adaptive features for future biologic imaging. By this feature NM analyses present a more developed interest.

The continuing development of new and specific diagnostic and therapeutic tracers is one of the unique adaptive features of nuclear medicine and PET which will help maintain its role in clinical imaging and medicine.

The new PET studies with the glucose analogue fluorine-18-labelled deoxyglucose (FDG) have shown a great ability of detecting tumor foci in a variety of histological neoplasms such as thyroid cancer, breast, lung cancer, etc. The contribution of the whole body PET (**WBPET**) imaging technique in diagnosis is also important.

Nuclear Medicine images (PET, SPECT) are functional compared to the rest of different types of investigations that are mostly anatomical. In Nuclear Medicine, the image depends on the type of that special organ, due to the special tracer and due to the specific function of the respective cell (the radio-tracer fixation is made by specific mechanisms, membrane mechanisms – electrochemical gradient, Na^+-K^+ pump special molecules presence in the respective cell, etc.) and not in relation with the tissular density (in the case of X-ray image) or the protons density (MRI case).

Producing 3D imaging has become a necessary important improvement for the body examination (which is intrinsically three-dimensional), and a better diagnosis [1]. Such techniques provide important quantities of data ($128\times128\times128$ matrix of voxels), that have to be visualized conveniently, to allow interpretation. 3D viewing may help to establish spatial relationships that may not be obvious in 2D imaging.

2. Image Acquisition

2.1. Tomography

X-ray CT scanner principle is based on two stages:

1 - acquisition of information over a section of interest,

2- computer image reconstruction.

Data are obtained by illuminating the object with an emitting light under different viewing angles.

In X-ray CT, data are measures of the attenuation of a given X-ray beam after it passes through the object. It is then possible to reconstruct a map of the X-ray linear attenuation coefficient in the 2D selected slices of human anatomy. Similar principles have been exploited for MRI or Emission Tomography.

In fact, 3D images may be produced using stack of parallel slices obtained with any of the available modalities. We refer to these techniques as "false" 3D imaging. For example, a stack of parallel X-ray CT scans constitutes a "false" 3D image.

The inconvenient in such a technique is constituted by the acquisition long duration (proportional to the number of slices), difference of spatial resolution between slices, problems related to biological or patient motion. Consequently, 3D images have to be pre-processed: interpolation in the third direction, in order to get a similar resolution in the 3 directions and if possible motion compensation.

Contrary, "true" 3D imaging refers to the production of images using specific 3D acquisition devices. We describe some of the possibilities of "true" 3D imaging for the different modalities.

2.2. Principle of 3D X-ray Tomography (**CT**)

The principle of "true" 3D X-ray imaging is a direct extension of X-ray CT scanners imaging. Instead of a fan-beam X-ray source, a cone-beam X-ray source, is rotated around the patient body. Instead of 1D profiles of attenuation, data are now constituted of radiographs of the volume to be imaged under different angles of view.

The 3D image is then obtained by solving a 3D-reconstruction problem from 2D projections. Such devices are called cone beam scanners.

The first prototype of this type was the **DSR** (Dynamic Spatial Reconstruction). It was constituted of 14 X-ray sources arranged on a gantry rotating around the patient. The radiographs of the volume are displayed, digitized on a brightness intensifier and sent to the computer for reconstruction.

2.3. Principle of 3D Magnetic Resonance Imaging (**MRI**)

There exist several acquisition techniques in MRI. The most popular is referred as 2D FT since the image is simply reconstructed from a 2D Fourier Transform of the projections. In this case, the application of two gradients of Magnetic fields in two orthogonal directions allows the encoding of the image slice in phase and frequency. This principle may be easily extended to three dimensions. Recent 3D MRI devices propose the acquisition of 3D images as a routine.

2.4. Principle of 3D Emission Tomography (**PET**, **SPECT**)

In the gamma emission tomography, the body is injected with an isotope special dedicated to a certain disease and specific organ. The porter molecule assures the fixation of the gamma-emitting isotope only in the target organ, (in vivo), in the human body.

Emission Tomography provides maps of the distribution of the radioactive isotope in a slice. There are two types of techniques: SPECT (Single Photon Emission Tomography) and PET (Positron Emission Tomography).

In SPECT, counts of photons emitted in different directions are collected. The use of cone beam collimators enhances detector efficiency and allows for truly 3D imaging [4]. PET which yields image distribution of positrons within a slice, is based on the fact that the annihilation of a positron (when it interacts with an electron creates a pair of photons emitted at 180° from one another.

Coincidence detection by two detectors of two gamma-ray photons locates a positron-emitting nucleus on the line joining the detectors. Software packages as ICON, Sopha/SMV NXT data sets, DICOM, SEGAMI workstation are some of the existing nuclear medicine advanced tools.

3. Grey level co-occurrence or grey level spatial dependencies

Also named co-occurrence matrix [16], it characterizes differences on image structures by the help of a geometric relation between pixels with certain intensities. We detect the occurrence frequencies for two pixels, one of gray level i and another one j, being in a certain position reported to the first one.

Gray level co-occurrence (GLCO) may be expressed by a symmetrical matrix whose lines and columns are indexed depending on their gray levels and whose elements are the reminded frequencies.

The relative position of the two pixels is given by two variables: the d distance between the pixels and the δ angle made by the line that unifies the two pixels with the horizontal.

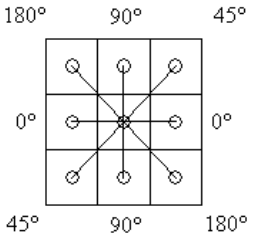

Fig. 1 – Pixels angles, in gray levels spatial dependence computing

Therefore, in a rectangular network there exists four possible relative positions for two pixels, therefore four co-occurrence matrix:

$$\mathbf{P}(i,\ j, d, 0^0) = \eta\{[(h, l), (m, n)] \left| k - m = 0, \right| l - n \left| = d \right.,$$

with $i = I(k,l),\ j = I(m, n)$ (1)

$$\mathbf{P}(i,\ j, d, 45^0) = \eta\{[(h, l), (m, n)] \left| (k - m = d, l - n = -d) \right.,$$

or $(k - m = -d, l - n = d)$, with $i = I(k, l),\ j = I(m, n)\}$ (2)

$$\mathbf{P}(i,\ j, d, 90^0) = \eta\{[(h, l), (m, n)] \left\| k - m \right| = d, l - n = 0,$$

with $i = I(k, l),\ j = I(m, n)\}$ (3)

$$\mathbf{P}(i,\ j, d, 135^0) = \eta\{[(h, l), (m, n)] \left| (k - m = d, l - n = d) \right.,$$

with $(k - m = -d, l - n = -d)$, with $i = I(k, l),\ j = I(m, n)\}$ (4)

where η represents the number of elements from the set, and $I(.,.)$ is the luminance in the specified co-ordinates point.

The matrix is symmetrical because $F(i,\ j, d, \delta) = F(j, i, d, \delta)$.

Table 1

Generic co-occurrence matrix

		"Grey" level			
		0	1	2	3
"Grey" level	0	η(0,0)	η(0,1)	η(0,2)	η(0,3)
	1	η(1,0)	η(1,1)	η(1,2)	η(1,3)
	2	η(2,0)	η(2,1)	η(2,2)	η(2,3)
	3	η(3,0)	η(3,1)	η(3,2)	η(3,3)

From the four matrix corresponding to the δ angle value, we may compute by mediation another resulting matrix, $\mathbf{P}(i, j, d)$ describing the relations of a pixel with all its neighbors (not depending on δ angle this time).

$$\mathbf{P}(i, j, d) = [\mathbf{P}(i, j, d, 0^0) + \mathbf{P}(i, j, d, 45^0) + \mathbf{P}(i, j, d, 90^0) + \\ + \mathbf{P}(i, j, d, 135^0)]/4 \tag{5}$$

We present the co-occurrence matrix associated to the two hemispheres calculated on an image selected from a nuclear medicine image database, for specific brain disfunctioning. The observable differences between the two cerebral hemispheres are expressed by the differences between the co-occurrence matrix.

We apply a variable threshold value in order to isolate significant difference matrix elements. The value might be automatically changed or may be chosen by the physician.

$$T(i, j) = \begin{cases} M(i, j) & abs(M(i, j)) > threshold \\ 0 & abs(M(i, j)) \le threshold \end{cases} \tag{6}$$

That is, for the upper matrix the low intensity colors (blue), are concentrated in a higher proportion into the right hemisphere, and the high intensity colors (yellow, red) are concentrated into the left hemisphere.

A *fuzzy variable threshold segmentation method* of treating the co-occurrence values is another appropriate mode of dealing with this global appreciation.

0.7629	0.0053	0	0	0	0	0	0
0.0053	0.0625	0.0046	0	0	0	0	0
0	0.0046	0.0366	0.0038	0	0	0	0
0	0	0.0038	0.0228	0.0042	0	0	0
0	0	0	0.0042	0.0434	0.0044	0	0
0	0	0	0	0.0044	0.0272	0	0
0	0	0	0	0	0	0	0
0	0	0	0	0	0	0	0

Fig. 2 – Left hemisphere co-occurrence matrix

0.7575	0.0058	0	0	0	0	0	0
0.0058	0.0878	0.0042	0	0	0	0	0
0	0.0042	0.0366	0.0053	0	0	0	0
0	0	0.0053	0.0491	0.0032	0	0	0
0	0	0	**0.0032**	**0.0270**	0.0009	0	0
0	0	0	0	**0.0009**	**0.0033**	0	0
0	0	0	0	0	0	0	0
0	0	0	0	0	0	0	0

Fig. 3 – Right hemisphere co-occurrence matrix

The difference co-occurrence matrix offers relevant indices on the presence of different degrees of radiotracer and isotope fixation on functional brain lobs.

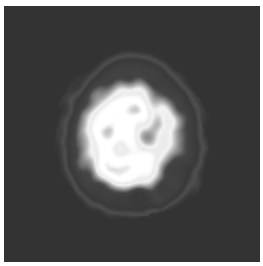

-0.0054	0.0005	0	0	0	0	0	0
0.0005	**0.0253**	-0.0003	0	0	0	0	0
0	-0.0003	0.0000	0.0015	0	0	0	0
0	0	0.0015	**0.0263**	-0.0011	0	0	0
0	0	0	-0.0011	**-0.0164**	-0.0035	0	0
0	0	0	0	-0.0035	**-0.0240**	0	0
0	0	0	0	0	0	0	0
0	0	0	0	0	0	0	0

Fig. 4 – The difference co-occurrence matrix

For a numerical quantification we may use the norm of the difference matrix defined by the singular value of the matrix. The performances obtained with GLCO method are due to the fact that the relations between the "gray" (pallet colors) levels of the pixels are statistical evidenced. This is in fact a statistical method of the second degree due to the interrelation between two pixels used. By generalization, a spatial dependence of "gray" levels for three or more pixels might be considered [2], [5].

4. Image positioning

Even if the images are centered by the gamma camera acquisition system, in order to compare the pixels corresponding to the two hemispheres, a more accurate central position is necessary. In this reason we detect on each line of our image, the exact position of pixels that bound the brain surface and stocks this information in a vector $V(N \times 2)$ where N represents the image height.

We calculate the medium values of all the pixels pairs and related to this we compute the straight line equation that approximates as good as possible these medium position values.

Obtaining such a straight line fit and knowing that the obtained line had to be a vertical line set exactly in the middle of the image we may compute a correction angle Φ, *if the image is obliquely positioned* [3].

After verifying and applying this angular position correction algorithm (if the case), we may compute Δx, that specifies the difference between the middles of the two lines, and we may realize a horizontal image translation.

A more complex method consists in finding the best-fitting ellipse approximating the brain outline [17] and then using the ellipse center as the center of the brain slice, and the orientation of the major axis gives the correction angle Φ.

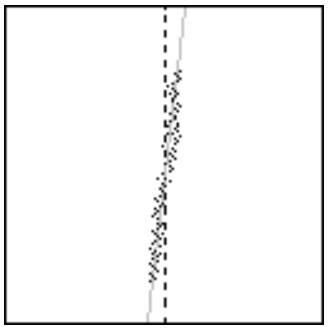

Fig. 5 – Straight line computing

5. Dis-functionality detection with variable threshold

Brain diagnosis differs from other organ diagnosis because it is done as a comparison between the normally symmetric left and right hemispheres of the brain. This makes very important to precisely find the center of the brain in each slice image and then to re-center each image accordingly.

A direct method to compare the two hemispheres is to make a difference between the gray levels of symmetric pixels in the two halves of a slice image. To the resulting matrix a threshold is applied to select the more interesting regions from the point of view of asymmetry.

The value of the threshold has to be determined based on a physician decision.

A fuzzy threshold is even more convenient for the diagnosis process. This method highlights the regions in the brain where the principle of symmetrical activity is not respected.

The physician is given the desfunctionality regions in the two hemispheres of the brain.

Fig. 6 – An image and the corresponding difference matrix for a brain slice

The next step is to compute the volume of such regions [1], [4] (selected also by the physician) and then to 3D reconstruct them. Determining the traces of the selected regions in consecutive slices until all the slices containing parts of the regions are determined is implied.

Another condition to validate a tumor region is to test the degree of radiopharmaceutical fixation in that region. Tumor regions have a low fixation degree that corresponds to the lower part of the color palette used to display the slice images (black or dark-blue in our examples).

Also a lower fixation degree can suggest double tumor regions in the case they are symmetric in the two hemispheres, case not detected by the above-described method. The low fixation test is implemented as a local maximum and minimum value detection algorithm.

Every slice image is scanned line by line and a graph of the gray level is computed for each line. Then maximum and minimum values are detected and a fuzzy threshold is applied to detect regions with radiopharmaceutical fixation lower than normal or imposed by a physician.

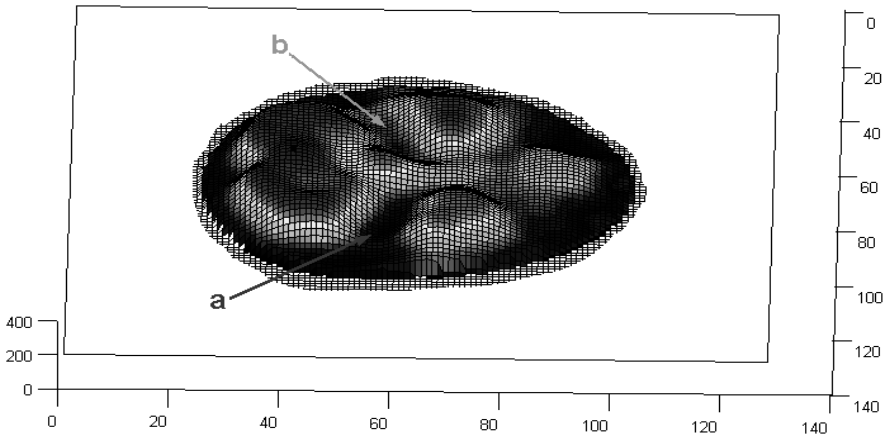

Fig. 7 – Dysfunctional area (a – possible tumor) enhanced by "false" 3D view representation, reported to its symmetric normal area (b).

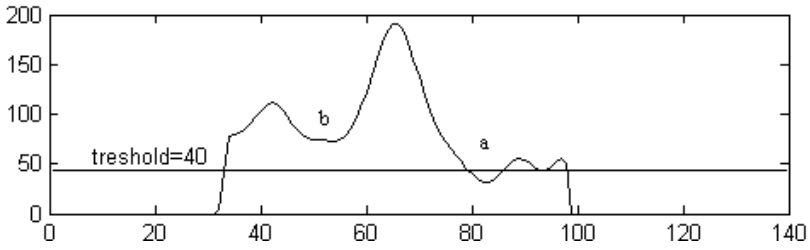

Fig. 8 – Interest zone cross-section for previous image.

Even if in Fig. 9 there is an evident asymmetry, the cross-section detects a different kind of radiotracer fixation denoting a partial dysfunctionality.

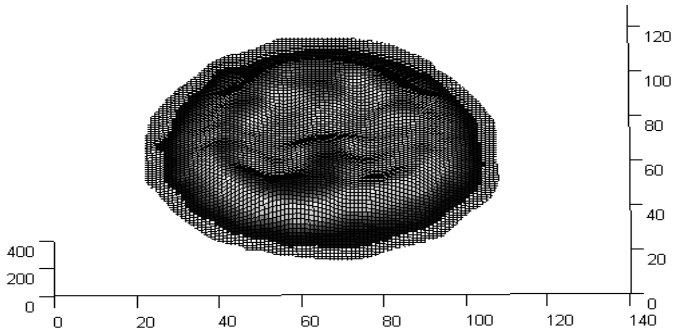

Fig.9 – Another dysfunctional area (not a tumor)

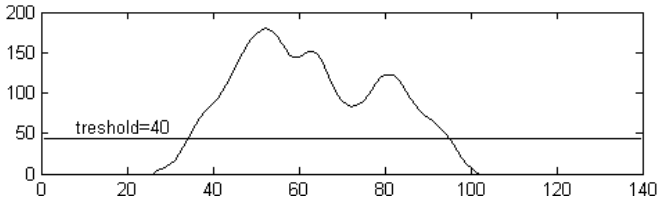

Fig. 10 – Interest zone cross-section for image represented in Fig.9.

6. 3D Images Displays

Assuming that we have a 3D image (i.e. a 3D $N \times N \times M$ matrix of "voxels", where $N \times N$ is the number of pixels in each slice and M is the number of slices). If M is not equal to N, the 3D matrix may first be pre-interpolated in order to obtain an image with an isotropic resolution. Traditional method for a partial visualization of 3D matrix is to display some of its 2D slices. It is straightforward to display slices along the three directions of the 3D matrix (transverse, sagittal and coronal slices).

Oblique slices in arbitrary directions may also be computed. A cut plane may define them, requiring some interpolation processes. In order to help in the representation, the cut plane may be represented on the whole 3D image. However this technique does not completely use all the available information [18] and it only provides a limited display of 3D images.

It is also important to have the possibility of projection visualization as they permit to have powerful indications on the 3D image

The method of using the maximum (or minimum) intensity projections (MIP) implies that the projection value as a given point is the maximum (or minimum) value of the 3D image on the straight line (This technique is very efficient for the visualization of blood vessels in MRI.

6.1. Surface Rendering

The surface of one or more particular structure(s) within the object may be displayed by this method. The definition of the surface, which is the method basis, relies on a segmentation step. It may be done by different means, either manually by an operator, either automatically using 2D or 3D-edge detection, or semi-automatically with a supervised contour detection [2]. Semi-interactive B-spline surface representations have first been proposed in [18].

If the segmentation step does not provide a model of the surface, it has to be constructed. It can be done using Besier curves, splines [16] or polyhedral approximation [3]. One of the most popular techniques is to represent the surface as a set of triangular patches. Defining these patches from the contours is called the process of triangulation. Triangulation methods [4], proposed in the literature are classified in two sets: optimal and heuristic methods. Optimal methods provide the best triangulation with respect to a given criterion (for instance, maximal volume polyhedron, minimal area polyhedron).

The problem is then expressed as seeking a minimal cost path in a graph, representing the set of all possible arrangements of the triangular patches (it proved to be a computationally expensive method). Heuristic methods consist of defining the triangular patches one by one using only a local decision criterion (method computationally less expensive than the previous one).

In non-convex contours, multiple branching, these methods can fail and we find an alternative method in [4] where is proposed an automatic heuristic triangulation algorithm giving solutions for single and multiple branching of contours even if they are very dissimilar in shape and orientation. The method uses a hierarchical procedure for decomposing a contour in terms of its convex and concave parts in order to link non-convex contours.

It may be displayed under different viewing angles using hidden surface algorithm (for instance, depth-buffer algorithm), including or not shading effects. Shading is obtained by applying an "illumination model". The resulting shade on a patch may be the combination on different phenomenon: ambient light, diffusion and reflection, refraction, etc.

A conventional model is Phong shading model:

$$I = I_a k_a + I_p (k_d \cos\theta + k_s \cos^n \alpha) \tag{7}$$

where I_a is the ambient intensity light, I_p the light intensity, θ is the angle between the surface normal and the direction of the light, and α is the angle between the reflection direction and the viewer. This model contains three terms: the first one is related to ambient light, the second one to diffusion and the third one to reflection. The constants k_a, k_r and k_s represent the contribution of each phenomenon on the image. Note that the angle θ is dependent of the normal to the surface at the considered point.

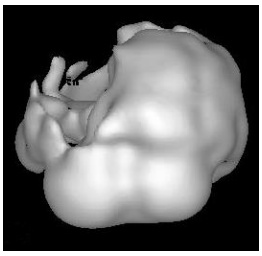

Fig.11 – 3D brain reconstruction containing a deep functional anomaly example

(DICOM web-site)

7. Conclusions

In imagistic medical diagnosis the proposed methods proved to be a reliable one providing an accurate delimitation of pathological radiotracer uptakes. This automatic method is a successfully decision aid one, partially replacing, assisting the classical manner of evaluation.

The accurate quantification of radiotracer uptake is improved by the presented method. In the case of tumoral SPECT, this quantification is decisive for the tumoral malignity degree, being demonstrated for gliomas, for example, that some radiotracers (^{201}Tl, ^{99m}Tc MIBI) [9], [14] are uptake in relation with the malignity. A volumetric quantification is more appropriate in relation with quantification on a reconstructed section.

Our method practically helped establishing a radiotracer uptake and/or distribution in order to determine with a higher accuracy the pathologic pattern, in diagnosis decision, for a same type of lesion.

References

[1] K.H. HOHNE, M. BOMANS, A. POMMERT, M. RIEMER, C. SCHIERS, G. WIEBECKE: *3D technique of tomographic volume data using the generalized voxel model, the visual computer*, vol. **6**, pp. 28-36, Springer-Verlag, 1990.

[2] R.M. HARALICK, L.G. SHAPIRO: *Computer and Robot Vision*, Addison-Wesley, vol. **2**, pp. 453-470, 1993.

[3] T.M. COVER: *Geometrical and Statistical Properties of Systems of Linear Inequalities with Applications in Pattern Recognition*, IEEE Trans. on Electronic Computers, vol. **14** (1965), pp. 326-334.

[4] A. EKOULE, F. PEYRIN, C. ODET: *A triangulation algorithm from arbitrary shaped multiple planar contours*, ACM Trans. on Graphics, vol. **10** (2), pp. 182-189, April 1991.

[5] S.-T. BOW: *Pattern Recognition and Image Preprocessing*, Marcel Dekker, Inc., N.Y., 1992.

[6] W.K. PRATT: *Digital Image Processing*, John Wiley & Sons, Inc., New York, 1991.

[7] K.C. HOH, CH. SCHIEPERS, A.M. SELTZER: *PET in Oncology: Will it Replace the Other Modalities?* in Seminars in Nuclear Medicine, Leonard M. Freeman and M. Donald Blaufox, Editors, The role of Nuclear Medicine in Oncological Diagnosis (Part 2), A Division of Harcourt Brace & Company, pp. 94-105.

[8] W.E. TRYCIECKY, A. GOTTSCHALK, K. LUDEMA: *Oncologic Imaging: Interactions of Nuclear Medicine with CT and MRI Using the Bone Scan as a Model*, in Seminars in Nuclear

Medicine, Leonard M. Freeman and M. Donald Blaufox, Editors, The role of Nuclear Medicine in Oncological Diagnosis (Part 2), W.B. Saunders Company, A Division of Harcourt Brace & Company, pp. 142-152.

[9] C. ŞTEFĂNESCU: *Medical Biophysics*, Tehnopress, Iaşi, 2002, pp. 282-294.

[10] C. ŞTEFĂNESCU, V. RUSU: *Radiopharmaceuticals Cellular Uptake Mechanisms*, Roumanian Journal of Biophysics, 1996, vol. **6**, 1-2, pp. 110 - 121.

[11] V. RUSU, C. STEFANESCU, M. MEIGNAN, L. CHOSSIERE, J. BON: *Imagistic Assessed of Astrocytoma Histologic Pattern Using ^{99m}Tc MIBI SPECT*, 1st Balkan Congress of Oncology, Athens, pp. 54, 1996.

[12] C. ŞTEFĂNESCU, V. RUSU, M. MEIGNAN, C. BADIU, F. ŞTEFANACHE: *^{99m}Tc MIBI in Neurofibromatosis Imaging Diagnosis*, The European J. of Nuclear Medicine, 1997, vol. **24** (8), 1029, (European Association of Nuclear Medicine Congress, Glasgow, 1997).

[13] R. GUCALP, JANICE P. DUTCHER, H.P. WIERNIK: *Overview by an Oncologist: What are the Imaging Needs of the Oncologist and Oncological Surgeon?*, in Seminars in Nuclear Medicine, Leonard M. Freeman and M. Donald Blaufox Editors, The role of Nuclear Medicine in Oncological Diagnosis (Part 1), A Division of Harcourt Brace & Company, pp. 3 - 9.

[14] C. STEFANESCU, M. MEIGNAN, V. RUSU: *Intêret de l'imagerie scintigraphique au ^{99m}Tc MIBI pour le diagnostic des gliomes*, Rev. Med. Chir. Soc. Nat., Iaşi, 1995, vol. **99** (3-4), pp. 99 - 107.

[15] www.segamicorp.com

[16] H.W. PRESS, A.S. TEUKOLSKY, T.W. VETTERLING, P.B. FLANNERY: *Numerical Recipes in C*, Cambridge University Press, 1994.

[17] A. FITZGIBBON, M. PILU, R.B. FISHER: *Direct Least Square Fitting of Ellipses*, IEEE Transactions on Pattern Analysis and machine Intelligence, vol. **21**(5), pp. 476-480.

[18] J. SEQUEIRA: *Modélisation interactive d'objets de forme complexe a partir de données shétérogenes*, Thése de doctorat d'Etat en Sciences, Besançon 1987.

Paper presented in a preliminary form in the **Second European Conference on Intelligent Systems and Technologies**, **ECIT'2002**, *Iasi, July 17-20, 2002*.